JABFM
eISSN 2280-8000

J Appl Biomater Funct Mater 2017; 15(1): e77-e83
DOI: 10.5301/jabfm.5000319

ORIGINAL RESEARCH ARTICLE

Anisotropy in the viscoelastic response of knee meniscus cartilage

Luca Coluccino[1,2], Chiara Peres[1], Riccardo Gottardi[3,4], Paolo Bianchini[1], Alberto Diaspro[1], Luca Ceseracciu[1]

[1] Nanophysics Department, Istituto Italiano di Tecnologia, Genoa - Italy
[2] IEIIT Institute, National Research Council of Italy, Genoa - Italy
[3] Department of Orthopaedic Surgery, Center for Cellular and Molecular Engineering, University of Pittsburgh, Pittsburgh, Pennsylvania - USA
[4] Ri.MED Foundation, Palermo - Italy

ABSTRACT

Background: The knee meniscus is instrumental to stability, shock absorption, load transmission and stress distribution within the knee joint. Such functions are mechanically demanding, and replacement constructs used in meniscus repair often fail because of a poor match with the surrounding tissue. This study focused on the native structure–mechanics relationships and on their anisotropic behavior in meniscus, to define the target biomechanical viscoelastic properties required by scaffolds upon loading.

Methods: To show regional orientation of the collagen fibers and their viscoelastic behavior, bovine lateral menisci were characterized by second harmonic generation microscopy and through time-dependent mechanical tests. Furthermore, their dynamic viscoelastic response was analyzed over a wide range of frequencies.

Results and conclusions: Multilevel characterization aims to expand the biomimetic approach from the structure itself, to include the mechanical characteristics that give the meniscus its peculiar properties, thus providing tools for the design of novel, effective scaffolds. An example of modeling of anisotropic open-cell porous material tailored to fulfill the measured requirements is presented, leading to a definition of additional parameters for a better understanding of the load transmission mechanism and for better scaffold functionality.

Keywords: Anisotropy, Biomechanics, Knee, Second harmonic generation microscopy, Stress relaxation

Introduction

The menisci are 2 wedge-shaped, semilunar, glossy white fibrocartilaginous tissues located between the femoral condyle and the tibial plateau. The main functions of the menisci are to increase congruency of shape between the curved condyle and the flat tibial plateau, to maintain stability and to bear and transfer load within the knee joint.

During activities of daily life, high compressive forces up to 3-4 times body weight are transferred via the surfaces of the femoral condyles and tibial plateau (1). The wedge-shaped meniscus distributes up to 90% of the axial load homogeneously over the tibial plateau, thus avoiding peaks of stress that may cause premature degeneration of the articular cartilage (2, 3). Moreover, the meniscus has a shock-absorbing capacity; a direct measure by Fukubayashi and Kurosawa (4) showed that, after removal of the meniscus, shock absorption was reduced by approximately 20%.

The mechanism of load transduction is based on the translation of a vertical compressive action into circumferential hoop stresses within the tissue (5, 6). To effectively transmit such loads, bundles of highly aligned collagen fibers run through the tissue between insertion sites on the tibial plateau, with other radial fibers that keep the overall structure packed under mechanical load.

Such structures give to cartilage a viscoelastic response to compressive viscoelastic loading, thanks to the flow of the interstitial fluid and the associated frictional drag. Upon loading with a constant or dynamic displacement, meniscal cartilage displays immediate elastic deformation controlled by the fluid pressurization in the interstitial matrix space (5). Then, if a constant strain is maintained, the fluid is expelled gradually from the matrix, and the stress is gradually relaxed. As displacement is removed, fluid reenters the tissue to recover the initial equilibrium. The viscous drag during each such cycle, arising from fluid movement and the intrinsic viscosity of cartilage, induces the dissipation of energy, which physiologically protects the articulation (7-9).

Accepted: May 30, 2016
Published online: September 14, 2016

Corresponding author:
Luca Ceseracciu
Istituto Italiano di Tecnologia – Smart Materials
Via Morego 30
16163 Genova, Italy
luca.ceseracciu@iit.it

Consequently, studying the effect of repetitive dynamic loads on articular cartilage similar to those occurring during daily activities, such as in walking and running, provides useful parameters to characterize the biomechanics of native tissue characterization (10).

In the case of meniscal damage, the effective reparation or replacement of these load-bearing structures must meet a number of requirements regarding force transmission and integration of the constructs with surrounding tissues. Following the perspective of Guilak et al on the role of biomechanics in tissue engineering (11), the success of an implant depends on some key aspects:

- defining standards of success for tissue repair;
- understanding the native tissue's biomechanical properties;
- prioritizing specific biomechanical properties as design parameters;
- the in vivo measurement of biomechanical parameters to provide in vitro regenerative models.

Although mechanical characterization of menisci has been the object of many studies (12-14), translation to substitutive medicine has been limited in 2 aspects (15): the tests performed are often time-consuming, and the deformation models are not explicit, therefore they do not provide simple parameters that can guide the design of scaffolds. Moreover, anisotropy in its mechanical properties, which is a key parameter for the meniscus, is rarely considered in the design of scaffolds that mimic and couple with native tissue.

In this study, we evaluated the stress-relaxation response of meniscus cartilage in unconfined compression, measuring compressive stiffness and stress relaxation. We studied the anisotropy of native bovine menisci collagen fibers and their relation to the biomechanical behavior of the tissue, with the final objective of guiding the efforts of meniscal cartilage regeneration, thus extending an approach already applied to few examples of scaffold design (16, 17). To that aim, we extracted simple parameters connected to key biomechanical properties, to provide a benchmark for scaffold validation and iterative optimization. We related the biomechanical characterization to the structural morphology of the tissue through second harmonic generation (SHG) microscopy and have provided guidelines for design of anisotropic scaffolds.

Finally, we evaluated the elastic shock absorption capability of native meniscus by assessing the energy dissipation across a wide range of frequencies by dynamic mechanical analysis, a technique often used to evaluate proper dissipation functioning (18) as well as long-term performance (19) of scaffolds and tissues. We highlighted the meniscus fibrocartilage frequency-dependent response in conditions that mimic physiological, dynamic activities.

Methods

Sample preparation

Bovine lateral menisci (n = 3) were obtained within 6 hours of animal sacrifice and maintained in a solution of phosphate-buffered saline (PBS; Sigma Aldrich) with 5% of streptomycin and penicillin at 4°C until sample preparation. Each meniscus was cleaned from other connective tissue and carefully divided into 3 macro regions: anterior horn, posterior horn and a central portion (Fig. 1A). From each region, a cuboid with 10-mm sides was extracted. To study the functional anisotropy of meniscus biomechanical features, each test was performed along 3 axes: the vertical (labeled as V), radial (R) and circumferential (C) (Fig. 1A), according to the 3 main collagen fiber orientations within the tissue in a polar coordinates system.

Second harmonic generation microscopy

SHG microscopy exploits a second-order nonlinear coherent optical process to image macromolecules with noncentrosymmetric structure, such as collagen fibers (20, 21).

Here SHG microscopy was used to investigate the hierarchical structure, organizational motifs and orientation of collagen fibers in the central portion of the bovine meniscus along each of the 3 polar axes (vertical, radial and circumferential). To perform SHG measurements, samples were fixed using formalin and cryosectioned into 8-µm slides. Images were acquired with a femtosecond Ti:Sapphire Chameleon Ultra II laser (Coherent, Santa Clara, CA, USA) coupled with a Leica TCS STED-CW confocal microscope (Leica Microsystems, Mannheim, Germany). The mosaic of false colored images was created by assigning the green to the 2 photon emission (2PE) autofluorescence and magenta and cyan to the Backward Second Harmonic Generation (BSHG) and Forward Second Harmonic Generation (FSHG) signals respectively: the final, merged images gave a direct morphological characterization. All images were acquired using a 370-nm pixel size, a scan speed of 700 Hz with 32 line averages.

Biomechanical analysis

The cuboid specimens intended for the mechanical evaluation were stored without fixation at 4°C in a solution of PBS with 5% streptomycin and penicillin, and tested within 12 hours. Samples were tested in uniaxial unconfined compression in a dynamic mechanical analyzer (DMA; Q800; TA Instruments) with a submersion fixture filled with PBS at a temperature of 37°C. Each cuboid was first tested along the vertical axis, then each sample was flipped 90°, allowed to rest in PBS until complete tissue relaxation, which was confirmed by full recovery of the original dimensions. It was then tested along the radial collagen fiber axis. Finally, samples were flipped laterally 90°, and the procedure was repeated along the circumferential fiber axis. Two types of biomechanical tests were performed: a stress-relaxation test and a dynamic test.

For the stress-relaxation test, the strain ramp applied to the samples started after a preload condition of 0.1% strain, reaching a strain of 10% with 0.1%/min strain rate, and was held constant for 30 minutes. The stress-strain data from the loading ramp were used to extract the elastic modulus at maximum load E (Fig. 1B). The relaxation portion of the stress-relaxation curves was fitted using the

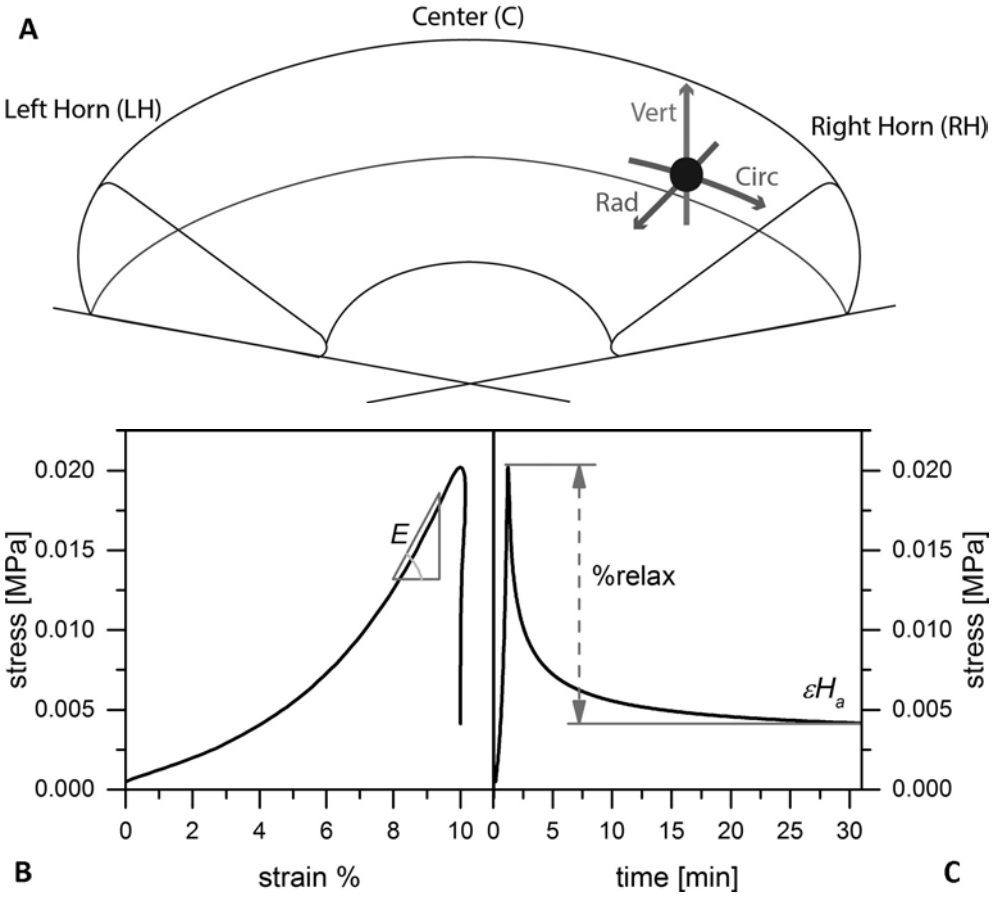

Fig. 1 - (**A**) Graphical representation of the triplet of axes (vertical, circumferential, radial) defined for the mechanical compressive analysis. (**B, C**) Typical curves from mechanical tests: stress-strain plot to evaluate the elastic compressive modulus E (**B**) and stress-relaxation curve as a function of time (**C**). The modulus at equilibrium H_a and the stress-relaxation capability were evaluated from the difference between the highest peak value and residual stress at the end of the test (30 minutes).

software Origin Pro 8.6 with the following nonlinear Prony series:

$$\sigma = \sigma_0 + A_1 e^{-\frac{t-t_0}{t_1}} + A_2 e^{-\frac{t-t_0}{t_2}} \quad \text{Eq. [1]}$$

Equation [1] was chosen for its good fitting of the experimental data and its general representation of viscoelastic materials, although it does not allow for the independent extraction of physical transient parameters. Nevertheless, it was possible to derive steady-state parameters, such as the equilibrium modulus at the end of the relaxation curve ($H_a = \sigma^{\infty}/\varepsilon$) and the relaxation percentage over the maximum stress (Fig. 1C). A_1, A_2 and t_0 were the fitting parameters.

The dynamic test of the meniscus cartilage consisted of a discrete frequency sweep from 0.1 to 40 Hz, applying a sinusoidal oscillating force of 0.01 N amplitude (on a static initial force of 0.1 N, corresponding to a strain amplitude of approximately 0.5%) in unconfined compression. Briefly, the displacement response was split in an in-phase and an out-of-phase component, from which the storage modulus (E') and the loss modulus (E") could be obtained, respectively. The ratio of the loss to the storage moduli is the tangent of the phase angle δ (tanδ) and represents the energy lost upon deformation, and is therefore connected to the dampening properties of the meniscus.

Results and discussion

Second harmonic generation microscopy

The morphological analyses performed by SHG microscopy showed the hierarchy of the collagen fiber bundles, highlighting the anisotropy of the native meniscus tissue (22-24). The SHG images (Fig. 2) allowed a detailed visualization of collagen fiber orientation on the 3 different planar sections. The collagen bundle orientation was clearly random in the first superficial layers of the meniscus cartilage (Fig. 2A), and the fiber bundles were qualitatively smaller in diameter, creating a homogeneous surface with the tribological properties required during gait when the femoral condyle slides on the meniscus (25). The radial planar section showed, instead, a high density of tightly packed circumferential collagen bundles with noticeably larger diameter (~100 µm) (Fig. 2B) and an essentially unidirectional alignment along the circumferential direction, which is instrumental in bearing the hoop stresses generated by vertical compressive loads (26). Finally, the SHG vertical planar section image clearly shows the arboreal organization of the radial fibers that "tie together" the meniscus, guarantee general tissue stability under the heavy vertical mechanical stress within the knee joint (27) and provide essential anchoring for the connective tissues around the outer meniscal perimeter.

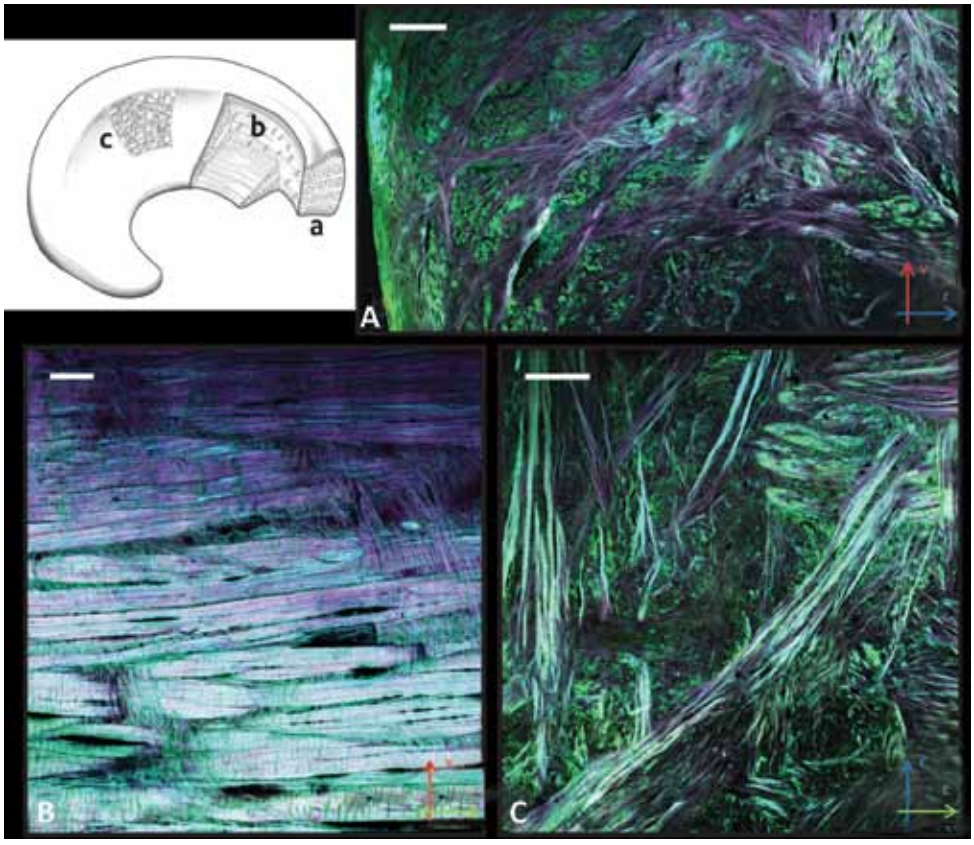

Fig. 2 - Sketch (upper left) of the different morphological regions of the meniscus, highlighting the collagen fiber bundle alignment: (**A**) Second harmonic generation microscopy (SHG) image of circumferential plane, (**B**) radial plane and (**C**) vertical plane section, each defined by the perpendicular direction. In each image green is the 2PE autofluorescence, magenta is the BSHG and cyan is the FSHG. Vertical (red), radial (light blue) and the circumferential (green) axis are reported on the plane sections. Scale bars = 200 μm.

Biomechanical analysis

The objective of this characterization was to provide mechanical parameters representative of native meniscus and of its anisotropy, to then tailor the mechanical design of substitute scaffolds. Bovine meniscus can be considered a multiphasic structure in terms of its mechanical response; hence, the experimental data were fitted to a Prony series with good agreement (R^2>0.995 in all cases). In our analysis we considered the meniscus as 1 orthotropic material, so as to characterize its mechanical response with the fewest possible parameters. The elastic response was found to depend on the compression axis (Fig. 3A-C), with higher values of the elastic modulus along the vertical axis, which can be explained by the higher linear density of collagen fibers along that direction.

The equilibrium modulus, proportional to the residual stress within the specimen at the end of the relaxation period, was significantly higher in the circumferential direction than in the radial one, with an intermediate, not significantly different, value in the vertical direction.

The stress relaxation was larger along the vertical axis (88%), while the C and R directions presented similar values. This suggests that, although the internal tissue matrix offers a higher vertical stiffness, according to the compressive modulus in the vertical direction, the collagen fiber packing structure allows a more efficient fluid exudation along the perpendicular directions, both radial and circumferential. The ensuing change of shape would reduce the stresses on the tibial plate and femoral condyle during sustained load (28). Moreover, the pressure driving fluid exudation is higher in the V direction, due to the higher stiffness.

These biomechanical responses can be interpreted in accordance with the morphology of the collagen fiber orientation within the native tissue evidenced by SHG microscopy. The presence of large circumferential bundles allows easier fluid exudation, so that relaxation along the perpendicular directions (vertical and radial) is higher. Furthermore, the stress-relaxation capability was not statistically different along the radial and vertical axes, and in fact, in both cases, the collagen architecture was similar, leading to comparable viscoelastic behaviors.

We characterized the dynamic response of bovine meniscus fibrocartilage by mimicking the physiological compressive stress levels and loading frequencies, with a special focus on the phase angle between applied sinusoidal stress and strain response, reported as tani, to evaluate the shock absorption capability of meniscus fibrocartilage.

The storage modulus E' for the 3 orientations is reported in Figure 3D. From the lowest frequency (0.1 Hz) to the highest (40 Hz), absolute values increased about 50%, with a fairly linear dependence of the frequency logarithm. This is a normal behavior for materials below the glass transition temperature, because of the reduced time for the material and fluid to respond to the imposed strain (29).

Orientation-wise, the modulus along the circumferential direction was higher, albeit not significantly, than that along the radial and vertical directions. Interestingly, static

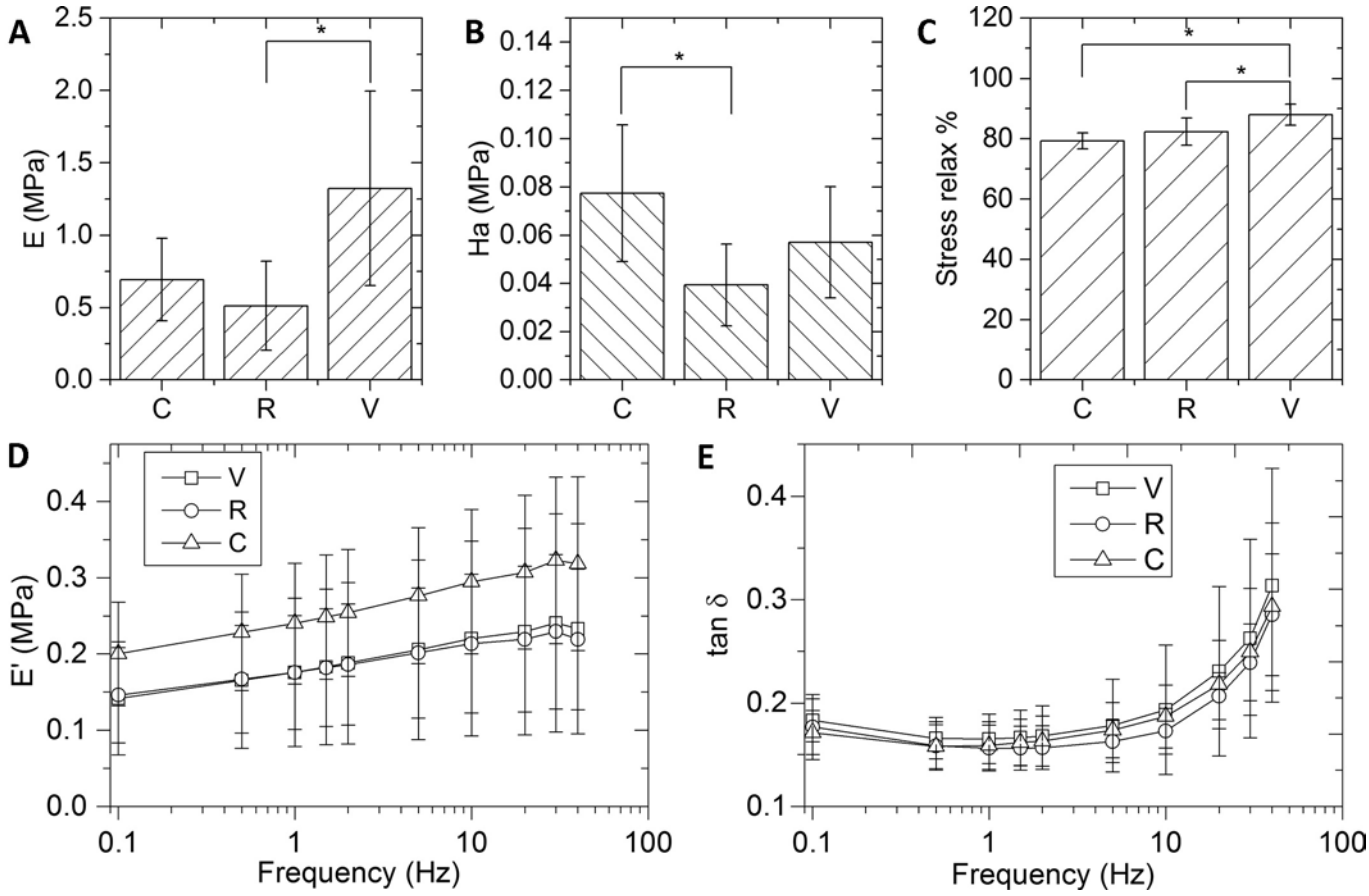

Fig. 3 - Summary results from the stress-relaxation test analyses along the circumferential (C), radial (R) and vertical (V) directions: (**A**) compressive modulus E; (**B**) equilibrium modulus H_a; (**C**) percentage stress relaxation. Error bars represent the standard deviation; *p<0.05. (**D, E**) Results from the dynamic mechanical analysis: (**D**) storage modulus E'; (**E**) tanδ as a function of frequency. Data represent the means of 3 specimens; error bars indicate the standard deviation.

measurements yielded a different ranking, with the vertical direction as the stiffest. This can be explained considering the different strain level, lower than 1% in dynamic tests: the thick collagen bundles deputed to tensile resistance were not subjected to buckling, like at 10% strain. Vertical orientation, for the same reason, did not benefit from the stress translation into hoop stress and offered, therefore, comparable stiffness to the structurally similar radial direction.

From the graph in Figure 3E, it is clearly visible that the values of tan increased significantly for frequencies above 10 Hz. A similar, although less pronounced, behavior was present at lower frequencies (<0.5 Hz). The increasing value of tane at higher frequencies was consistent with the meniscal physiological dampening function (22). In fact, higher frequencies (above 10 Hz) meant rapid deformations such as those occurring during jumping or impacts, which require the dissipation of excess energy to protect the underlying musculoskeletal tissues, whereas at frequencies corresponding to normal physiological dynamics, conservative deformations (low tanp) reduce the energy dispersed in common movements, especially walking.

In other words, meniscal cartilage is naturally designed to respond to frequencies dangerous for other joint tissues, and acting as a smart material, it dissipates energy via redistribution of the bulk stress and fluid pressurization levels (1). Orientation-wise, there are no marked differences in the tan. for the 3 loading directions. This suggests that the small amplitude applied during testing is not affected by fluid exudation and is therefore not dependent on specific structures of collagen bundle orientations.

From these mechanical characterizations, it is possible to devise a theoretical design procedure for synthetic scaffolds centered on mimicking the functional behavior of native meniscus without having to necessarily replicate its natural structure. In this way, starting from a chosen bulk material, the morphology of the scaffold can be tailored to meet the mechanical requirements and their anisotropy.

As a relatively simple example, let us consider an open-cell orthotropic porous material in which pores are treated as ellipsoids. For a given value of porosity , the anisotropy of the pores can include differences in the diameter along each direction (D_c, D_R, D_V) and in the area of the throats between pores along each direction (A_c, A_R, A_V), as shown in Figure 4. We can define the ratios between pairs of diameters and throat areas as $R_{ij} = D_i/D_j$ and $R'_{ij} = A_i/A_j$, respectively.

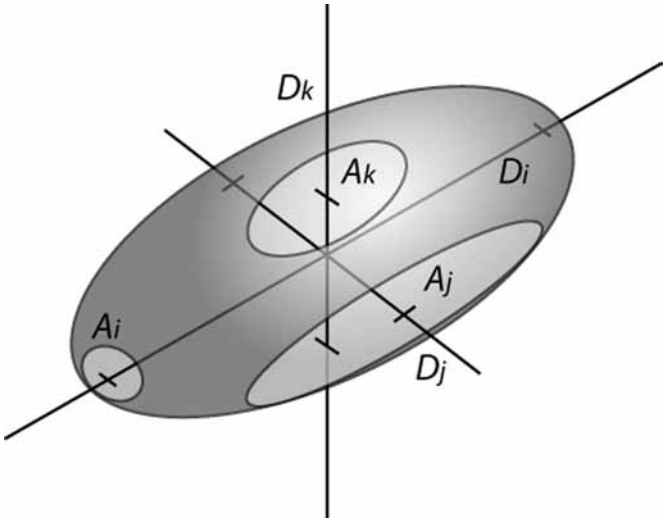

Fig. 4 - Example model of a single cell in an anisotropic porous material. The key parameters affecting the mechanical anisotropy are shown: *D* indicates the pore diameter and *A* the throat area along each coordinate (i, j, k).

Assuming that the stress relaxation is due mainly to fluid exudation, we can take the percentage of stress relaxation as the target porosity of our scaffold. This indeed is not strongly affected by the load direction:

$$\varphi \approx \% \, relax \qquad \text{Eq. [2]}$$

From the number of pores and their shape, it is possible, conversely, to optimize the material selection, in terms of bulk modulus E_b and bulk density , to match the porosity (30):

$$E^* \sim E_b \rho (1-\varphi) \qquad \text{Eq. [3]}$$

In case of anisotropic cells, the moduli ratio follows the geometrical one as:

$$R_{ij}^2 \approx \frac{E_i}{E_j} \qquad \text{Eq. [4]}$$

From this equation, the pore ratios can be estimated.

The equilibrium modulus H_a can be linked to the scaffold permeability, as shown by Vikingsson et al (31) for confined compression tests, through the relaxation time and scaffold thickness h:

$$H_a = \frac{h^2}{\pi^2 \tau k} \qquad \text{Eq. [5]}$$

Equation [5] can not be applied directly to unconfined compression tests, for the difference in the fluid path and the stress state. Nonetheless, the proportionality between equilibrium modulus and permeability stands; since permeability is proportional to the cross-sectional area (32), which in turn is proportional to the throat area of a single pore, the permeability anisotropy is equal to:

$$R'_{ji} \approx \frac{H_{ai}}{H_{aj}} \qquad \text{Eq. [6]}$$

TABLE I - Physical and anisotropic geometrical parameters of a model scaffold based on the viscoelastic characterization of native meniscus

E_b (MPa)	4.5	R_{RV}	0.62
ϕ	0.83	R'_{CR}	0.51
R_{CR}	1.16	R'_{CV}	0.74
R_{CV}	0.72	R'_{RV}	1.45

E_b = bulk Young's modulus; ϕ = porosity.

From these considerations, a candidate scaffold can be proposed, with the physical and geometrical properties as reported in Table I, choosing a typical polymer density of 1.1 g/cm^3.

This theoretical design tool does not take into account other aspects, not connected directly to mechanical properties, such as the ideal pore size for cell proliferation and nutrient diffusion.

It provides, nonetheless, indications for a starting geometry to be optimized in successive iterations, to meet the requirements identified ex vivo. It is worth stressing that mechanical validation is based on empirical parameters that can be obtained by a single test along each direction, in a simple setup of unconfined compression.

A more exhaustive characterization, useful to predict the performance of the scaffold once implanted, includes the response of the constructs to dynamic loading. Although dynamic properties are more difficult to directly correlate to structure, knowledge of the response of native tissues to a broad range of dynamic stimuli, representative of different physiological activities, can provide the target against which to characterize the response of proposed meniscal substitutes.

Conclusion

In this study, we characterized native meniscus in terms of elastic and viscoelastic parameters, such as the compressive modulus and the stress-relaxation capability, evidencing the anisotropy of the biomechanical response along polar coordinates. Morphological characterization was achieved by SHG microscopy, one of the most promising techniques to investigate anisotropic collagen-based tissues, which provided structural details in support of the mechanical functional mapping.

Overall, our results were both in good agreement with the known meniscus load transfer functions and consistent with the organization of collagen fibers. Along the vertical direction, stiffness was higher to withstand higher loads thanks to the higher collagen bundle linear density, whereas stress at equilibrium was lowest to allow adaptation to the tibial plate and femoral head.

Our overall characterization offers a functional tool for the design of scaffold that takes into account the anisotropic structure of the native tissue. With regard to an approach to repairs, this characterization provides a useful baseline for the design of implants for knee meniscus substitution and for scaffolds for meniscal tissue engineering with high functional biocompatibility.

Acknowledgement

The authors would like to thank Mr. Federico Parodi, Sant'Olcese (GE), for kindly providing the bovine meniscal tissues. R.G. wishes to acknowledge the Ri.MED Foundation, Palermo, Italy, for its support.

Disclosures

Financial support: No grants or funding have been received for this study.
Conflict of interest: None of the authors has any financial interest related to this study to disclose.

References

1. Martin Seitz A, Galbusera F, Krais C, Ignatius A, Dürselen L. Stress-relaxation response of human menisci under confined compression conditions. J Mech Behav Biomed Mater. 2013;26: 68-80.
2. Kutzner I, Heinlein B, Graichen F, et al. Loading of the knee joint during activities of daily living measured in vivo in five subjects. J Biomech. 2010;43(11):2164-2173.
3. Seedhom B. Transmission of the load in the knee joint with special reference to the role of the menisci: Part I: anatomy, analysis and apparatus. Eng Med. 1979;8(4):207-219.
4. Fukubayashi T, Kurosawa H. The contact area and pressure distribution pattern of the knee: a study of normal and osteoarthrotic knee joints. Acta Orthop Scand. 1980;51(6):871-879.
5. McDermott ID, Masouros SD, Amis AA. Biomechanics of the menisci of the knee. Curr Orthop. 2008;22(3):193-201.
6. Jones RS, Keene GC, Learmonth DJ, et al. Direct measurement of hoop strains in the intact and torn human medial meniscus. Clin Biomech (Bristol, Avon). 1996;11(5):295-300.
7. Fahlgren A, Johansson L, Edlund U, Aspenberg P. Direct ex vivo measurement of the fluid permeability of loose scar tissue. Acta Bioeng Biomech. 2012;14(2):47-51.
8. Costa A. Permeability-porosity relationship: a reexamination of the Kozeny-Carman equation based on a fractal pore-space geometry assumption. Geophys Res Lett. 2006;33(2):L02318.
9. Marsano A, Wendt D, Raiteri R, et al. Use of hydrodynamic forces to engineer cartilaginous tissues resembling the non-uniform structure and function of meniscus. Biomaterials. 2006;27(35): 5927-5934.
10. Suh JK, Li Z, Woo SLY. Dynamic behavior of a biphasic cartilage model under cyclic compressive loading. J Biomech. 1995; 28(4):357-364.
11. Guilak F, Butler DL, Goldstein SA. Functional tissue engineering: the role of biomechanics in articular cartilage repair. Clin Orthop Relat Res. 2001;391(Suppl):S295-S305.
12. Lai JH, Levenston ME. Meniscus and cartilage exhibit distinct intra-tissue strain distributions under unconfined compression. Osteoarthritis Cartilage. 2010;18(10):1291-1299.
13. Chia HN, Hull ML. Compressive moduli of the human medial meniscus in the axial and radial directions at equilibrium and at a physiological strain rate. J Orthop Res. 2008;26(7):951-956.
14. Haut Donahue TL, Hull ML, Rashid MM, Jacobs CR. How the stiffness of meniscal attachments and meniscal material properties affect tibio-femoral contact pressure computed using a validated finite element model of the human knee joint. J Biomech. 2003;36(1):19-34.
15. Buma P, Ramrattan NN, van Tienen TG, Veth RP. Tissue engineering of the meniscus. Biomaterials. 2004;25(9):1523-1532.
16. Esposito AR, Moda M, Cattani SM, et al. PLDLA/PCL-T scaffold for meniscus tissue engineering. Biores Open Access. 2013;2(2):138-147.
17. Balint E, Gatt CJ Jr, Dunn MG. Design and mechanical evaluation of a novel fiber-reinforced scaffold for meniscus replacement. J Biomed Mater Res A. 2012;100(1):195-202.
18. Silva-Correia J, Gloria A, Oliveira MB, et al. Rheological and mechanical properties of acellular and cell-laden methacrylated gellan gum hydrogels. J Biomed Mater Res A. 2013;101(12): 3438-3446.
19. Gloria A, Causa F, De Santis R, Netti PA, Ambrosio L. Dynamic-mechanical properties of a novel composite intervertebral disc prosthesis. J Mater Sci Mater Med. 2007;18(11):2159-2165.
20. Chen X, Nadiarynkh O, Plotnikov S, Campagnola PJ. Second harmonic generation microscopy for quantitative analysis of collagen fibrillar structure. Nat Protoc. 2012;7(4):654-669.
21. Bianchini P, Diaspro A. Three-dimensional (3D) backward and forward second harmonic generation (SHG) microscopy of biological tissues. J Biophotonics. 2008;1(6):443-450.
22. Zhu W, Chern KY, Mow VC. Anisotropic viscoelastic shear properties of bovine meniscus. Clin Orthop Relat Res. 1994;(306): 34-45.
23. Abraham AC, Edwards CR, Odegard GM, Donahue TL. Regional and fiber orientation dependent shear properties and anisotropy of bovine meniscus. J Mech Behav Biomed Mater. 2011;4(8):2024-2030.
24. Fisher MB, Henning EA, Söegaard N, Esterhai JL, Mauck RL. Organized nanofibrous scaffolds that mimic the macroscopic and microscopic architecture of the knee meniscus. Acta Biomater. 2013;9(1):4496-4504.
25. Hasan J, Fisher J, Ingham E. Current strategies in meniscal regeneration. J Biomed Mater Res B Appl Biomater. 2014;102(3): 619-634.
26. Fithian DC, Kelly MA, Mow VC. Material properties and structure-function relationships in the menisci. Clin Orthop Relat Res. 1990;(252):19-31.
27. Makris EA, Hadidi P, Athanasiou KA. The knee meniscus: structure-function, pathophysiology, current repair techniques, and prospects for regeneration. Biomaterials. 2011;32(30): 7411-7431.
28. Meakin JR, Shrive NG, Frank CB, Hart DA. Finite element analysis of the meniscus: the influence of geometry and material properties on its behaviour. Knee. 2003;10(1):33-41.
29. Menard KP. Dynamic mechanical analysis: a practical introduction. Boca Raton, FL: CRC Press; 1999.
30. Gibson LJ, Ashby MF. Cellular solids: structure and properties. 2nd ed. Cambridge, UK: Cambridge University Press; 1997.
31. Vikingsson L, Claessens B, Gómez-Tejedor JA, Gallego Ferrer G, Gómez Ribelles JL. Relationship between micro-porosity, water permeability and mechanical behavior in scaffolds for cartilage engineering. J Mech Behav Biomed Mater. 2015;48: 60-69.
32. Ho ST, Hutmacher DW. A comparison of micro CT with other techniques used in the characterization of scaffolds. Biomaterials. 2006;27(8):1362-1376.